Advances in Nanotechnology

Volume II

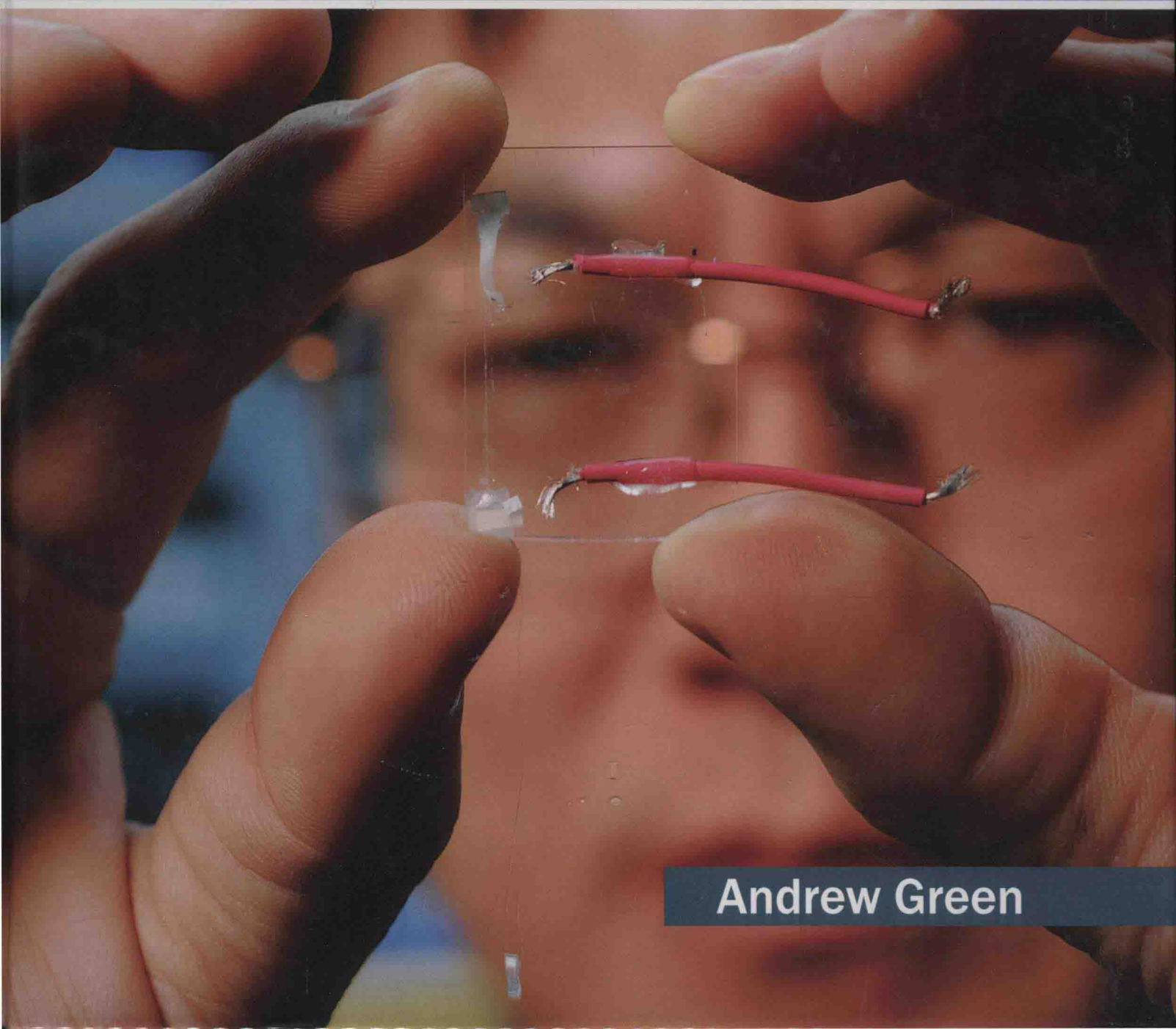

Andrew Green

Advances in Nanotechnology
Volume II

Edited by **Andrew Green**

NY RESEARCH
PRESS
New York

Published by NY Research Press,
23 West, 55th Street, Suite 816,
New York, NY 10019, USA
www.nyresearchpress.com

Advances in Nanotechnology: Volume II
Edited by Andrew Green

International Standard Book Number: 978-1-63238-036-4 (Hardback)

Printed in China.

Preface

This book is a compilation of research material on the emerging field of Nanotechnology. Engineering of functional systems at the molecular scale is referred to as nanotechnology or nanotech. Both the current work and advanced concepts related to this field are covered in this book. Nanotechnology is a technique used to construct an item using the bottoms up approach with high atomic precision. Today, by utilizing the technological advancement and techniques available in the field of nanotechnology, high performance products can be developed.

According to Feynman's vision of miniature factories, to build complex products using nanomachines, advanced nanotechnology should utilize positionally-controlled mechanochemistry guided by molecular machine systems. Nanotechnology is used in various fields of science these days. It plays a key role in areas such as medicine sciences, biotechnology etc. Besides, other applications include green nanotechnology, energy applications of nanotechnology and carbon tube related applications among numerous others.

This book provides a variety of researches and studies based on nanotechnology. It also covers some of the emerging aspects in the field of nanotechnology. I wish to thank all the authors for their efforts and time that they have given to this project. Without their dedication and timely submissions, this publication wouldn't have been possible. I must also acknowledge the editor and the team at the publishing house, who have done a tremendous job. Last but not the least, I wish to thank my family and friends, who have supported me in my life through everything. This book is meant for students, researchers, scientists, and for all those who want to learn and explore this interesting field of science.

Editor

Contents

Probing Phonons in Nonpolar Semiconducting Nanowires with Raman Spectroscopy

Kofi W. Adu,[1,2] Martin D. Williams,[3] Molly Reber,[3] Ruwantha Jayasingha,[3] Humberto R. Gutierrez,[4] and Gamini U. Sumanasekera[3,5]

[1] *Physics Department, Altoona College, Pennsylvania State University, Altoona, PA 16601, USA*
[2] *Materials Research Institute, Pennsylvania State University, University Park, PA 16802, USA*
[3] *Department of Physics & Astronomy, University of Louisville, Louisville, KY 40292, USA*
[4] *Physics Department, Pennsylvania State University, University Park, PA 16802, USA*
[5] *Conn Center for Renewable Energy Research, University of Louisville, Louisville, KY 40292, USA*

Correspondence should be addressed to Kofi W. Adu, cxa269@psu.edu

Academic Editor: Qihua Xiong

We present recent developments in Raman probe of confined optical and acoustic phonons in nonpolar semiconducting nanowires, with emphasis on Si and Ge. First, a review of the theoretical spatial correlation phenomenological model widely used to explain the downshift and asymmetric broadening to lower energies observed in the Raman profile is given. Second, we discuss the influence of local inhomogeneous laser heating and its interplay with phonon confinement on Si and Ge Raman line shape. Finally, acoustic phonon confinement, its effect on thermal conductivity, and factors that lead to phonon damping are discussed in light of their broad implications on nanodevice fabrication.

1. Introduction

Since the discovery of the Raman scattering process by Raman and Krishnan in 1928 [1] and the invention of the laser in 1960 by Maiman [2–4], Raman spectroscopy has morphed from standard macroprobe of bulk materials to single molecular detection [5–11]. The innovations in Raman spectroscopy have made it one of the most widely used techniques to probe nanostructures, beside transmission electron microscopy (TEM), scanning electron microscopy (SEM), X-ray diffraction (XRD), and atomic force microscopy (AFM) as shown in Figure 1. The data in Figure 1 was collected from the ISI web of science site for the period of January 1996 to July 2010 on nanoscale characterization tools used in probing nanostructures [12]. Even though probing individual nanostructures by Raman spectroscopy at nanoscale is limited by its low spatial resolution (diffraction limit of the objectives), recent developments in nano-Raman spectroscopy, including scanning near-field optical microscopy (NSOM), tip enhanced Raman spectroscopy (TERS), and surface enhanced Raman spectroscopy (SERS), have made single-molecule detection possible [5–11, 13–17], especially using SERS and TERS. While NSOM is based on the principle of optical tunneling of evanescent waves, TERS and SERS are based on excitation of surface plasmons on the surface of nanometals. The process arises when free electrons on the surface of a metal oscillate collectively in resonance with the oscillating electric field of the incident light wave. The interaction between the surface charge and the electromagnetic field helps concentrate the light on the surface of the metal, leading to electric field enhancement. Irrespective of such great innovative techniques in nano-Raman spectroscopy, nearly 84% (see Figure 1) of Raman characterization use conventional Raman spectroscopy to probe nanoscale samples [12]; that is, probing ensembles of nanostructures instead of individual nanostructures.

The dramatic surge in the use of Raman spectroscopy in probing nanostructures is mainly due to the immense information (such as amorphization, defects, sample temperature (local heating), size distribution, strain effects, phonon confinement, type of doping, phase separation, carrier concentration, and mobility) [24–38] that can be readily acquired

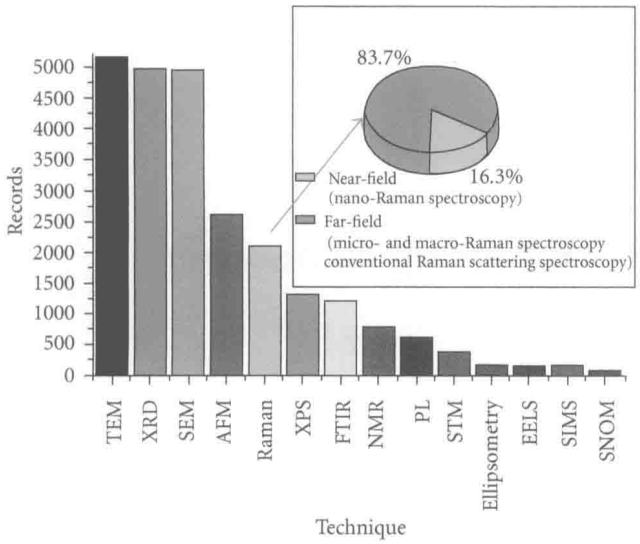

FIGURE 1: Number of records of the listed nanocharacterization tools used in probing nanostructures in the period of January 1996 to July 2010 (Source: ISI Web of Science, http://apps.isiknowledge.com/) [12].

from analysis of the peak-frequency and line width of the Raman profile. Additionally, (i) the nondestructive nature of the Raman probing technique, (ii) limited or no sample preparation, (iii) simultaneous *in situ* measurement, (iv) submicron spatial resolution when coupled with AFM (TERS) or SEM, and (v) very high sensitivity when coupled with surface enhanced/resonance spectroscopy have made Raman spectroscopy an easy-to-use instrument for quick sample screening. Thus, Raman spectroscopy has been used extensively to probe optical phonons, surface phonons, acoustic phonons, and antenna effects in nanowires.

In this paper, we concentrate on recent developments in optical and acoustic phonon confinement in nonpolar semiconducting nanowires, using Si and Ge; as examples, since many of the concepts that we discuss here are applicable to any related systems. Other phenomena in nanowires such as antenna effects and surface phonons are not covered here. In this chapter, we will review optical and acoustic phonon properties using Si and Ge nanowires as prototype and the new phonon dispersion due to radial (circumferential) confinement. Additionally, we will review physical properties such as thermal conductivity that are significantly influenced by phonon confinement.

Our understanding of the bulk properties of crystalline and amorphous Si and Ge continue to be of immense importance to the development of electronic, optoelectronic, photovoltaic, and other devices, as well as the society at large. The past two decades have seen scientific advances in low-dimensional systems by reducing the three-dimensional bulk system (3D) to two-dimensional thin-film systems (2D) to one-dimensional and quasi-one-dimensional (1D) systems of nanowires and nanotubes [39–64] and to zero-dimensional (0D) systems of quantum dots [39–41].

Following the growth of nanowires using pulsed laser vaporization in 1998, different synthesis techniques have been developed using the vapor-liquid-solid mechanism (VLS) [65–79]. These have led to intense research activities due to the unique properties of the nanowires compared to their bulk counterparts, and several applications of nanowires including sensors, transistor and logic gates, electrooptics, thermoelectric, photovoltaic, electrochemical capacitors, and batteries have been proposed. Most of these applications take advantage of quantum confinement effects at small diameters, which for Si and Ge occur at diameters $\leq$20 nm [44–47, 80]. Both theoretical [81–84] and experimental [83, 85–88] evidence of the effects of confinement on the electronic states of nanowires have been reported for Si and other nanowires [89–91]. These reports indicate a transition from indirect band gap to direct band gap in the nanowires where the band gap scales with diameter as $\sim D^{-1.7}$ [83, 84, 88, 92, 93]. Most studies of nanowires have focused on the electronic states; however, the importance of phonon states in nanowires cannot be overemphasized. Most of the electronic properties are intricately influenced by phonon scattering since it is the dominant scattering mechanism at high temperatures. The influence of phonon confinement, geometry, and surface roughness of nanowires on thermal conductivity, specific heat capacity, and electron mobility has been demonstrated theoretically and experimentally [94–101]. Different confinement models including lattice dynamic simulation [102] and spatial correlation (phenomenological) [12, 44–47, 80, 103–111] model have been used to calculate phonon dispersion and Raman line shape profiles of nanowires, respectively. We will discuss the phenomenological model later. However, readers who are interested in the lattice dynamic calculation should see [102].

Majority of the optical phonon confinement reports in the literature for semiconducting nanowires of (a) Si, Ge, (b) III-VI, II-VII compounds, and (c) oxide compounds have analyzed their results using the spatial correlation model developed by Richter and coworkers [106] and further extended by Campbell and Fauchet [107]. Application of this model to experimental data and the influence of laser flux on the Raman line shape will be discussed here.

Small diameter semiconducting nanowires exhibit phonon confinement due to the long length of the phonon wavevector q compared to the radius of the nanowire, which violates the $q = 0$ selection rule, permitting multiple wavevector of various $q < 1$ to contribute to the phonon linshape. Based on the spatial correlation model first proposed by Richter et al. [106] and expanded further by Campbell and Fauchet [107], it has been argued that restriction of the phonon wave function within a particle of size D results in an uncertainty $\Delta q \sim \pi/D$ in the phonon wavevector of the zone-center optical phonon and a corresponding uncertainty $\delta\omega$ in its wavenumber [112]. Consequently light scattering takes place from quasi-zone-center optical phonons with wavevector q up to π/D. This is in fact valid only for weak phonon localization and the effect diminishes as q approaches π/D [110].

Germanium and silicon belong to the cubic O_h^7 space group and crystallize into the ($F4_1/d32/m$) diamond lattice. The conventional lattice of diamond consists of two interpenetrating face-centered cubic (fcc) atomic lattices which

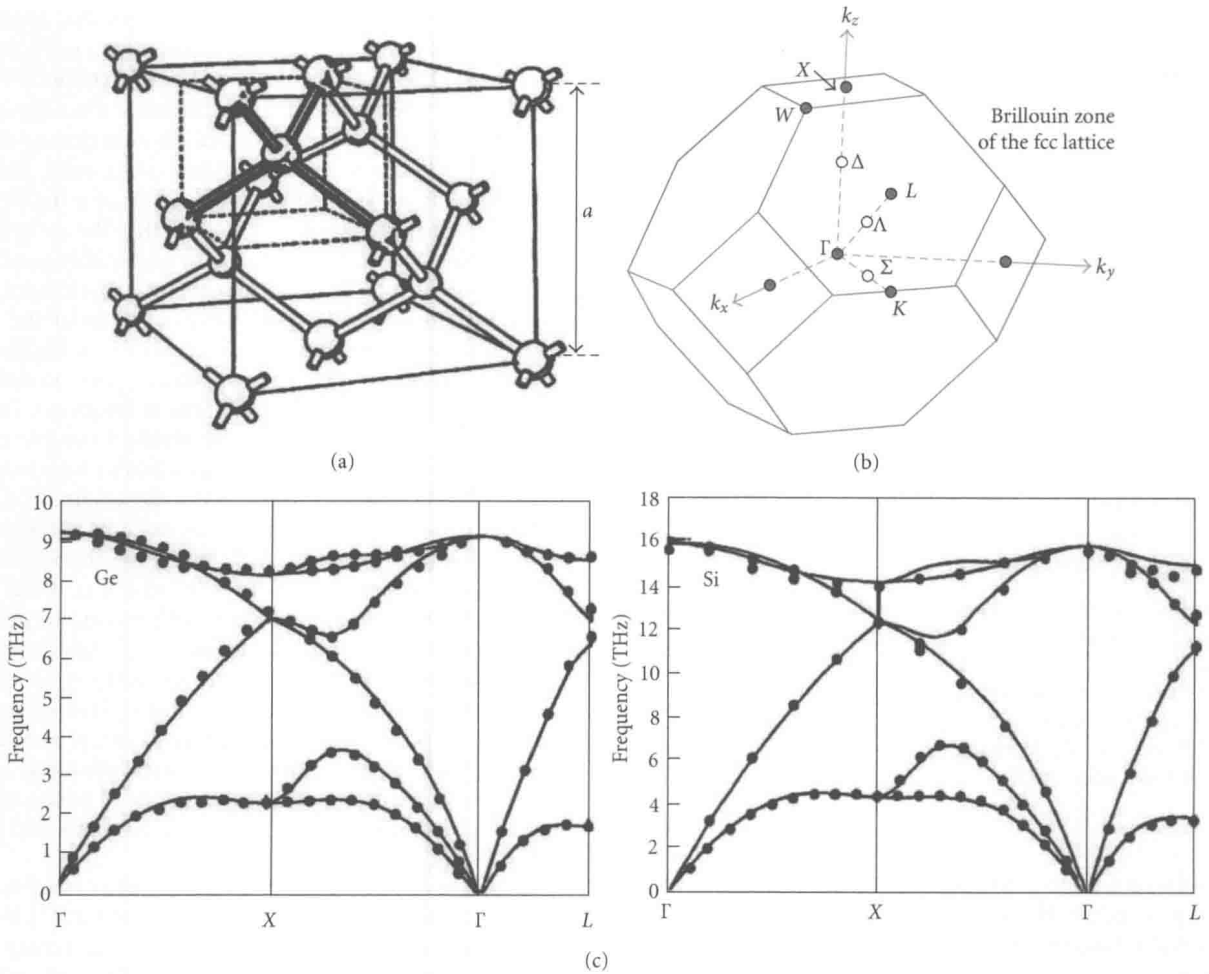

FIGURE 2: (a) Conventional cubic unit cell for the diamond crystal structure ($F4_1/d32/m$). Each atom is tetrahedrally bonded to four nearest neighbors. The lattice parameter of the conventional unit cell containing four atoms, $a = 0.5431$ Å (Si) and $a = 0.5658$ Å (Ge), (b) Brillouin zone for the face-centered space lattice showing the positions of several high-symmetry axes and points [18, 19]. (c) Phonon dispersion curves of Ge [20] (left) and Si [20] (right) along high-symmetry directions. The dots are neutron scattering data [19, 21, 22], and the solid lines are calculations using up to the sixth nearest neighbor interactions in a Born-von Kármán force constant model [20]. The primitive cell contains two atoms; therefore, three optical branches (2TO and 1LO) and three acoustic branches (2TO and 1LO) are observed. These branches are degenerate at the Γ point.

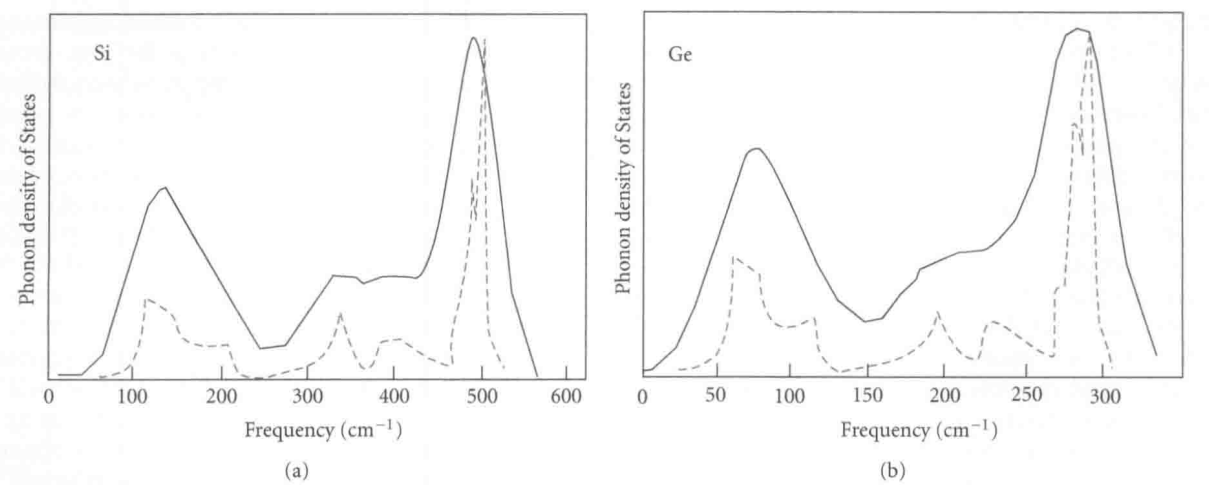

FIGURE 3: Calculated phonon density of state for Si (a) and Ge (b). Solid lines represent a highly disordered material, and the dashed lines represent the crystalline material [23].

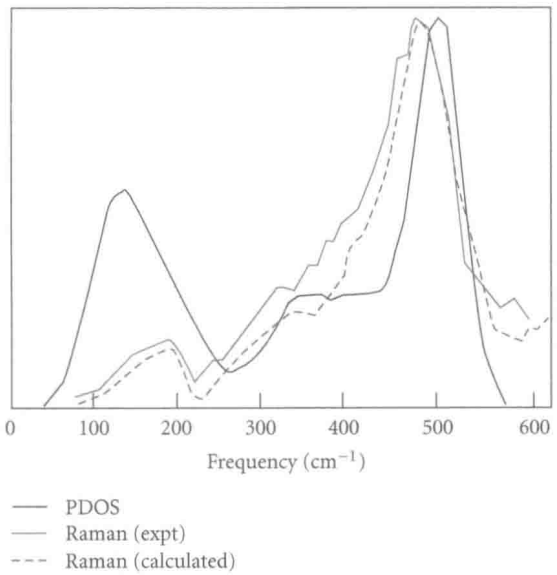

FIGURE 4: Comparison of experimental Raman profile (thin solid line) and calculated first-order Raman band of highly disordered Si (dashed line). The bold solid line is the calculated phonon density of states (PDOS) for highly disordered Si. The experiment and calculated Raman spectra are in good agreement. The difference in the PDOS and the calculated Raman band shows the importance of matrix element effects [23].

are displaced a quarter of the body diagonal of the conventional cubic cell with respect to each other. Each atom is tetrahedrally bonded to four nearest neighbors. The 3-dimensional unit cell of a tetrahedrally bonded diamond lattice is shown in Figure 2(a), and the corresponding Brillouin zone indicating the positions of several high-symmetry axes ($\mathbf{X}, \mathbf{L}, \mathbf{W}, \mathbf{K}$) and points ($\Gamma, \Lambda, \Delta, \Sigma$) is shown in Figure 2(b) [18, 117]. The phonon dispersion curves along some of these high-symmetry axes for crystalline Si and Ge, obtained from neutron scattering data [19, 21] (dots) and a fit to the data using (up to the sixth nearest neighbor) the Born-von Kármán force constant model (solid line), are shown in Figure 2(c) [19–22] right and left, respectively. At the points in the Brillouin zone where the phonon dispersion curves flatten, $d\omega/dk \sim 0$, and peaks appear in the phonon density of states. However, in highly disordered systems, these features in the phonon density of states are observed to be broadened. Shown in Figure 3 are the calculated phonon density of states for bulk Si (a) and Ge (b). The dashed and solid lines in the figure represent crystalline and highly disordered systems [23], respectively. Note that the disorder introduces both smearing of the sharp peaks in the phonon density of states and disappearance of the fine structures associated with the crystalline state; however, the three main broad features remain. Interestingly, strong disorder does not destroy the main features of the phonon density of states associated with the crystalline system.

If we compare the first order Raman spectra of disordered and crystalline Si, we observe a sharp Lorentzian peak at $\sim 520\,\text{cm}^{-1}$ of full width at half maximum (FWHM) of $\sim 4\,\text{cm}^{-1}$ for the crystalline state. Strongly disordered Si on the other hand exhibits a Raman spectrum that approaches the calculated phonon density of states shown in Figure 3(a). In this case, the peak at $\sim 520\,\text{cm}^{-1}$ now exhibits a FWHM of $\sim 100\,\text{cm}^{-1}$, that is, ~25 times broader than the crystalline bulk. In Figure 4, the calculated phonon density of states (thick solid line), Raman spectrum (thin solid line) and calculated Raman spectrum (dashed line) of a highly disordered Si are compared [23]. It is clear that the experimental and the calculated Raman data are in reasonably good agreement. It can also be inferred that the matrix element effects are important if a truly quantitative analysis of the data is desired. Nevertheless, the Raman spectrum of highly disordered system can provide very important phonon density of states information throughout the entire frequency range.

The first Brillouin zone is the smallest volume entirely enclosed by planes that are the perpendicular bisectors of the reciprocal lattice vectors drawn from the origin. The region in k-space that low-k phonons can occupy without being diffracted is called the first Brillouin zone. It contains phonons with k values from 0 to π/a, where a is the lattice parameter. For monoatomic solids with two atoms per primitive cell such as diamond, magnesium, Si, Ge, or diatomic compounds such as GaAs, there are three optic phonon branches in addition to the three acoustic phonon branches. In compounds with a greater number of atoms and complex crystal structures, the number of optical phonons is more than three. If the crystal unit cell contains N atoms, then $3N$ degrees of freedom result in 3 acoustic phonons and $3N - 3$ optical phonons.

Phonons can propagate in the lattice of a crystal as a wave and their dispersion depends on their wavelength [118]. For a given nanowire material, the confinement effects may exhibit different asymmetric broadening and shifts, depending on the symmetries of the phonon and their dispersion curves. There is also dependence on the excitation energy such that phonons of certain symmetry are more responsive to resonance conditions [119]. Transverse phonon confinement in nanowire is due to their one-dimensional geometry. The wavevector is unrestricted in the longitudinal (z) direction, but it is confined and quantized in the tangential (radial) direction as illustrated in Figure 5.

In bulk crystalline materials, Raman spectroscopy and other optical techniques can only probe zone center phonons. Absence of lattice periodicity in nanocrystalline materials relieves this $q = 0$ selection rule. In general, for semiconducting nanowires, phonon confinement is not the only effect linked to diameter. Electronic states of semiconducting-nanowires can be tuned via the wire diameter D, as the band gap should scale approximately as $1/D$ [120].

The organization of this chapter is as follows. We will discuss in Section 2 the spatial correlation phenomenological model for optical phonons and relate it to experimental data from Raman spectroscopy of confined optical phonons in Si and Ge nanowire in Section 3. In Section 4, we will discuss the influence of local inhomogeneous laser heating on the Raman profile of Si and Ge nanowire. Acoustic phonon confinement and its effect on thermal conductivity will be presented in Section 6 and Section 7 will be devoted to summary of the main points presented in this paper and suggestions for future research in phonon confinement.

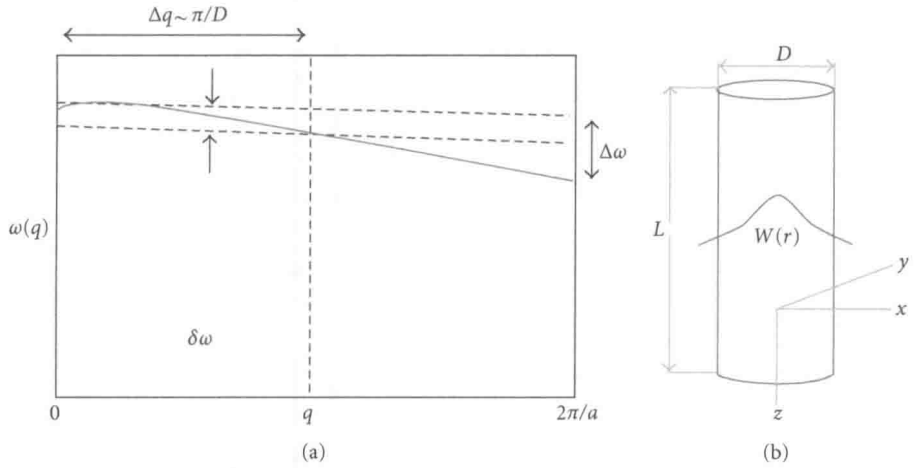

FIGURE 5: (a) Optical phonon dispersion $\omega(q)$ of Si with the first order Raman scattering phonon frequencies extend throughout $\Delta\omega$. Raman active wavevectors of a nanowire with diameter D lie within Δq. (b) Schematic of nanowire of diameter ($D = 2r$) and length L and the confined phonon wave function, $W(r)$.

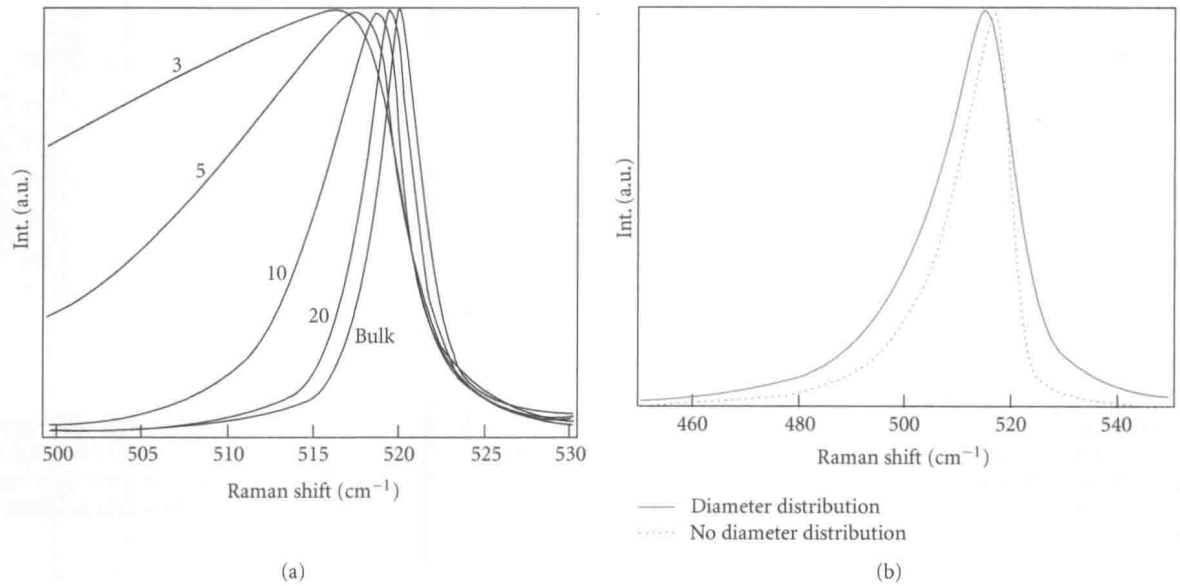

FIGURE 6: (a) A plot showing the finite-size-induced phonon confinement effect (downshift and asymmetric broadening to lower energy) for different diameters of Si nanowires and the Lorentzian line shape of the bulk, for comparison. (b) Comparison of the Raman line shape of 8 nm diameter Si nanowires, taking diameter distribution into account and without diameter distribution. The peak downshift ~1 cm^{-1} and the line width broadened ~30%.

2. Theoretical Models of Phonon Confinement in Nanowires

2.1. Spatial Correlation Model of Raman Scattering for Confined Optical Phonons in Nanowires. Richter and coworkers [106] were the first to propose a phenomenological phonon confinement model (sometimes called Richter model) to explain the experimental observation of a downshift and asymmetric broadening of the first-order Raman profile of crystalline nanostructures. Their approach naturally leads to relaxation of the conservation of the bulk crystal momentum in the scattering process. Assuming a spherical nanocrystalline shape and using the diameter as an adjustable parameter, they fitted the Raman line shape of a film of small Si nanocrystals. Their model was further extended by Campbell and Fauchet [107] who considered other nanocrystalline shapes (i.e., wires and platelets).

For Si and Ge, the longitudinal optic (LO) and the tangential optic (TO) modes are degenerate at the Γ point (zone center). Conservation of the phonon momentum in crystalline Si and Ge produces a Raman active mode of the optical phonons from only the zone center ($q = 0$) at 520 cm^{-1} and 300 cm^{-1} for Si and Ge, respectively. In nanowires, the transverse phonons are confined in the two orthogonal directions perpendicular to the nanowire axis. This allows a greater range of phonon modes to contribute to the Raman

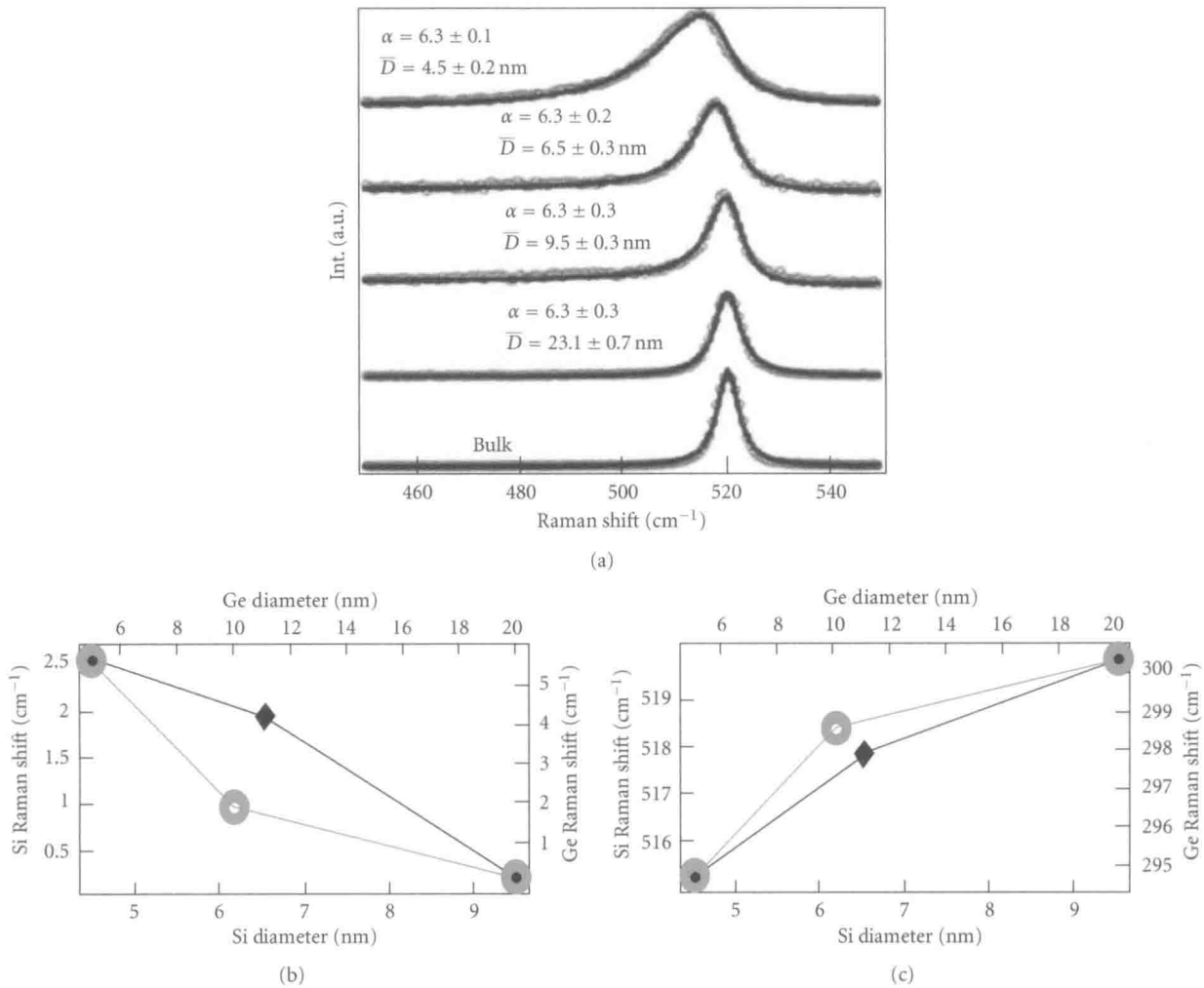

FIGURE 7: (a) Raman spectra showing the first-order Raman band peaks in four ensembles of Si nanowires. The bulk Si (001) spectrum is also shown. Experimental data: red open circles, least-square fit: black solid lines. α is the attenuation factor of the phonon (the width of the Gaussian phonon quantum confinement function) at the real boundary $r = D/2$, $\overline{D}$ is the most probable diameter. (b) Comparison of experimental Raman shift of TO phonon in Si [47] and Ge nanowires [80] for different diameters. Top: absolute shift Si (diamond), Ge (circles); bottom: nanowire Raman shift relative to bulk. Note that the Ge diameter range is twice that of Si.

scattering process. In fact, bulk phonons of wavevector up to $q \sim 1/D$ (D is diameter of the nanowire) contribute to the first-order Raman spectrum.

The Richter model line shape function of the first-order Raman profile of a nanowire expressed in terms of the transverse phonon wavevector ($q_\perp$) can be written as [44–47, 80, 104, 106, 107, 113, 121–123]

$$I_{NW}(\omega) = A_o \int_o^{q_{\max}} \frac{|C(0,q_\perp)|^2}{[\omega - \omega_o(q_\perp)]^2 + (\Gamma/2)^2} 2\pi q_\perp dq_\perp, \quad (1)$$

where A_o is an adjustable parameter, ω is phonon frequency measured relative to the laser line, $\omega_o(q_\perp)$ is the bulk transverse phonon frequency, Γ is the FWHM of the bulk phonon Raman profile, and $|C(0,q_\perp)|^2$ is the spectral weighting function expressed as

$$|C(0,q_\perp)|^2 \sim \exp\left[-\frac{1}{2}\left(\frac{q_\perp D}{\alpha}\right)^2\right], \quad (2)$$

D is the diameter of the nanowire and α is a dimensionless adjustable parameter. Figure 6(a) shows the evolution of the Raman profile with diameter ($20 \geq D \geq 3$) of the 520 cm^{-1} optical phonon of Si nanowire, calculated using (1). Here, $\Gamma = 4.5\ cm^{-1}$ and $\alpha = 6.3$ were used in the calculations [53]. Since most Raman scattering experiments are performed on ensembles of nanowires, any analysis using the Richter model should take into account the diameter distribution $F(D)$ of the ensemble nanowires. This modifies the Richter model by introducing a second integral due to the diameter distribution as

$$I_{NDW}\left(\omega, \overline{D}\right) = \int_o^\infty F(D) I_{NW}(\omega, D) dD, \quad (3)$$

where $\overline{D}$ is the ensemble most probable diameter and the rest of the parameters are as defined previously. Figure 6(b) shows a comparison of calculated Raman line shape of 8 nm Si nanowire with (solid line) and without (dash line)

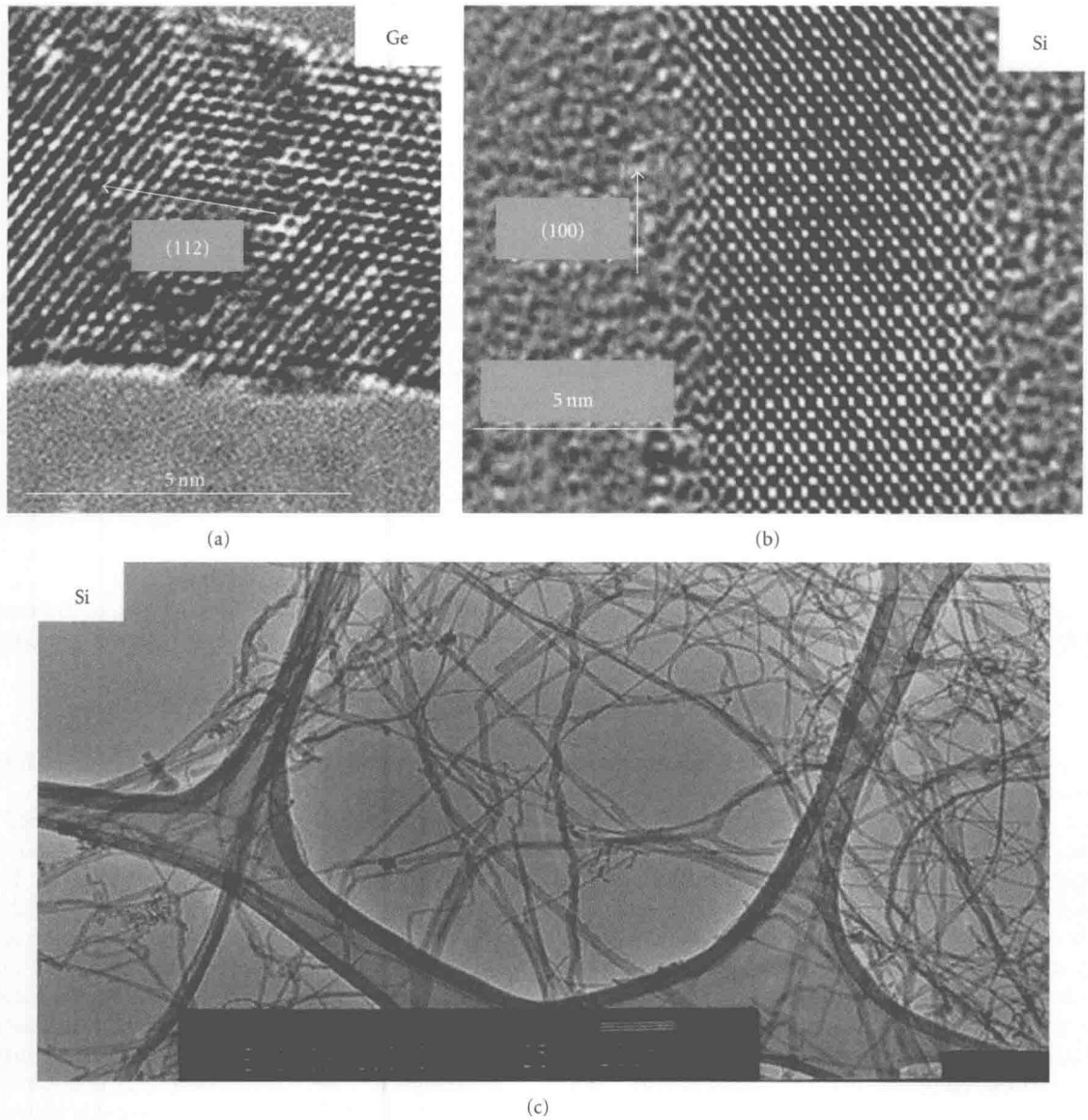

FIGURE 8: HRTEM images of (a) 6 nm diameter Ge nanowire [80], (b) 7 nm Si nanowire [47], and (c) LRTEM images of Si nanowires.

diameter distribution. There is a clear difference in the Raman profile of with and without the inclusion of the diameter distribution that demonstrates its importance in the interpretation of Raman spectra of confined phonons. It must be emphasized that the model is inconsistent at diameters ≤ 3 nm. This has been discussed in detail in [44–47].

3. Experimental Evidence of Confined Optical Phonons in Nanowires

Optical phonons propagate in the lattice of a single crystal as a wave and exhibit dispersion depending on their wavelength, or equivalently their wavevector in the Brillouin zone [118]. The momentum conservation selection rule determines the region of the Brillouin zone that can be accessed in the Raman scattering process. In a Raman scattering experiment, the magnitude of the scattering vector is $2k_o \sin(\theta/2)$, where k_o is the wavevector of the incident light and θ is the scattering angle. The maximum value of the scattering vector would be $2k_o$ (in the backscattering configuration), $\sim 5 \times 10^4\ \text{cm}^{-1}$ for visible light. Hence, this wavevector is much smaller than the wavevector q of the full phonon dispersion curve, which extends up to the boundary of the Brillouin zone ($\pi/a \sim 10^8\ \text{cm}^{-1}$). Since acoustic phonons mostly have very small wavenumbers, they could only be probed with Brillouin spectrometer consisting of a Fabry-Perot interferometer. Thus, only the optical phonons close to the zone centre ($q \approx 0$) are probed in visible Raman spectroscopy of bulk samples. This $q \approx 0$ selection rule is essentially a consequence of the infinite periodicity of the crystal lattice. However, if the periodicity of the crystal is curtailed, as in the case

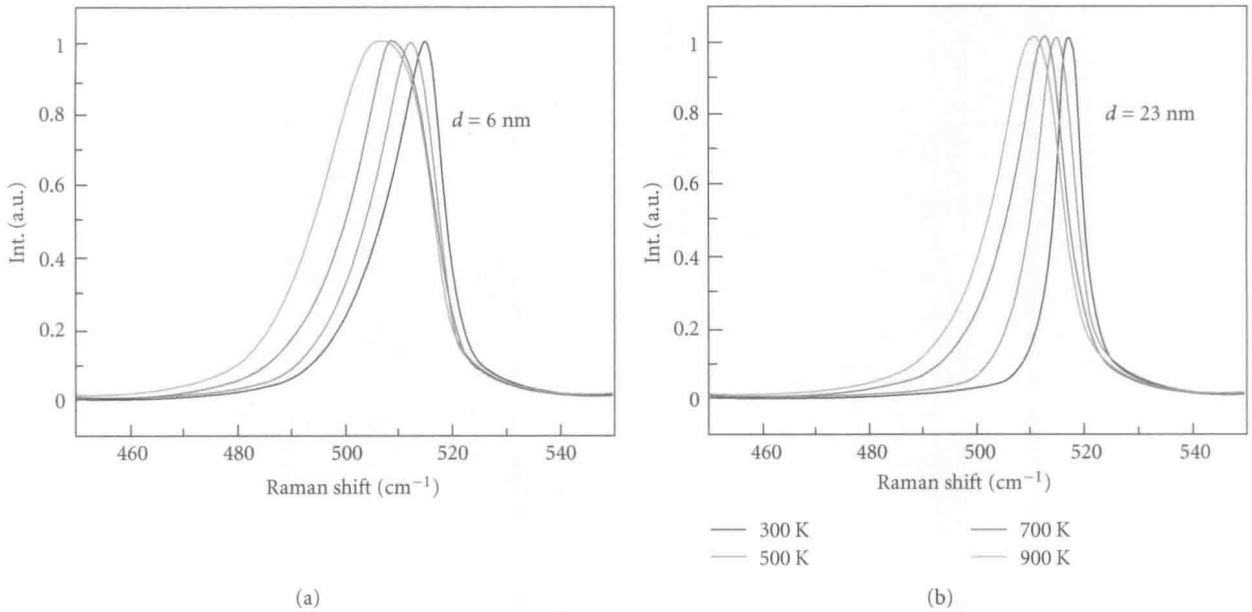

FIGURE 9: Calculated Raman line shape of the 520 cm^{-1} band of Si nanowires subjected to laser inhomogeneous heating. The focal spot size is 1 μm in the micro-Raman focal plane. Results are calculated using (10) at the different peak temperatures indicated for (a) $D = 6.0$ nm and (b) $D = 23$ nm nanowires [44–46].

of nanocrystalline materials, the $q \approx 0$ selection rule is relaxed, leading to asymmetric broadening and downshift in the Raman profile, in the case of Si and Ge.

Additionally, it has also been observed that, the supporting substrate plays an important role in Raman scattering experiment [44, 46, 80, 124]. If the supporting substrate is a poor thermal conductor, the Raman peak shift to lower frequency due to heating [44, 46, 80]. There is substantial evidence showing that both quantum confinement and inhomogeneous heating induce redshift and asymmetric broadening relative to the bulk, in Raman spectra of optical phonons in Si and Ge nanowires [44, 46, 122, 123, 125]. Here, we focus on phonon confinement of the first-order Raman spectrum in semiconducting nanowires of Si and Ge and would discuss the effect of inhomogeneous heating later.

3.1. Semiconducting Nanowires: Si and Ge. Si nanowire has always been the prototype for nanoscale semiconducting studies due to the vast information on its bulk counterpart. The earliest reports of phonon confinement in nanowire [106, 107] focused on Si. The shape and frequency of the Raman peaks due to scattering by the optical phonons are thought to be dependent on the diameter of the nanowire. The onset of phonon confinement is at the point where the phonon mean free path is comparable to the diameter of the nanowire [47]. Figure 7(a) shows the first systematic report on the evolution of Raman spectrum of Si nanowires with diameters for 3 nm $\leq$ D $\leq$ 20 nm. The open circles represent the raw Raman data, and the solid line is a least square fit of the Richter model including diameter distribution (3). It depicts an asymmetric broadening to lower frequency and a downshift as reported by Adu and coworkers [47]. Similar arguments can be made for Ge nanowires which have been reported by Jalilian and coworkers [80].

Figures 7(b) and 7(c) are the plots of measured TO optical phonon peak frequency, versus Si and Ge nanowire diameter [47, 80]. The solid line is a guide to the eye. These plots show a significant difference between Ge and Si TO phonons. In the absolute shift case, the Si slope between 4.5 and 9.5 nm is 0.9086 cm^{-1}/nm and the Ge slope between 5 and 10 nm is 0.7634 cm^{-1}/nm. As the nanowire diameter decreases, the absolute Raman shift of the TO phonon increases but the Raman shift relative to the bulk decreases, in accordance with the theory [47]. The Ge nanowire TO phonon apparently only reaches bulk-like behavior at a diameter between 10 and 20 nm whereas for silicon this occurs between 5 and 10 nm. Both Ge and Si nanowires exhibit TO phonon confinement that induces an absolute Raman shift over a range of 5 cm^{-1} [47, 80]. The ranges of Raman shift relative to bulk, however, are approximately 2.6 and 7 cm^{-1} for Si and Ge, respectively. Although the absolute Raman shift of both Si and Ge shows positive curvature with nanowire diameter, the curvature is negative for Ge in the relative shift. It should be noted that the excitation laser wavelength used in Figures 7(b) and 7(c) is nearly in resonance with the Si sample but far from it for the Ge sample.

4. Effect of Inhomogeneous Laser Heating on Confined Optical Phonons

Typically, the laser irradiation during Raman measurements can cause sample heating and photon excitation of charge carriers [104, 126–130]. Downshifting and broadening of Raman bands in bulk materials, with increasing laser radiation, is typically identified to be due to laser heating. Poor

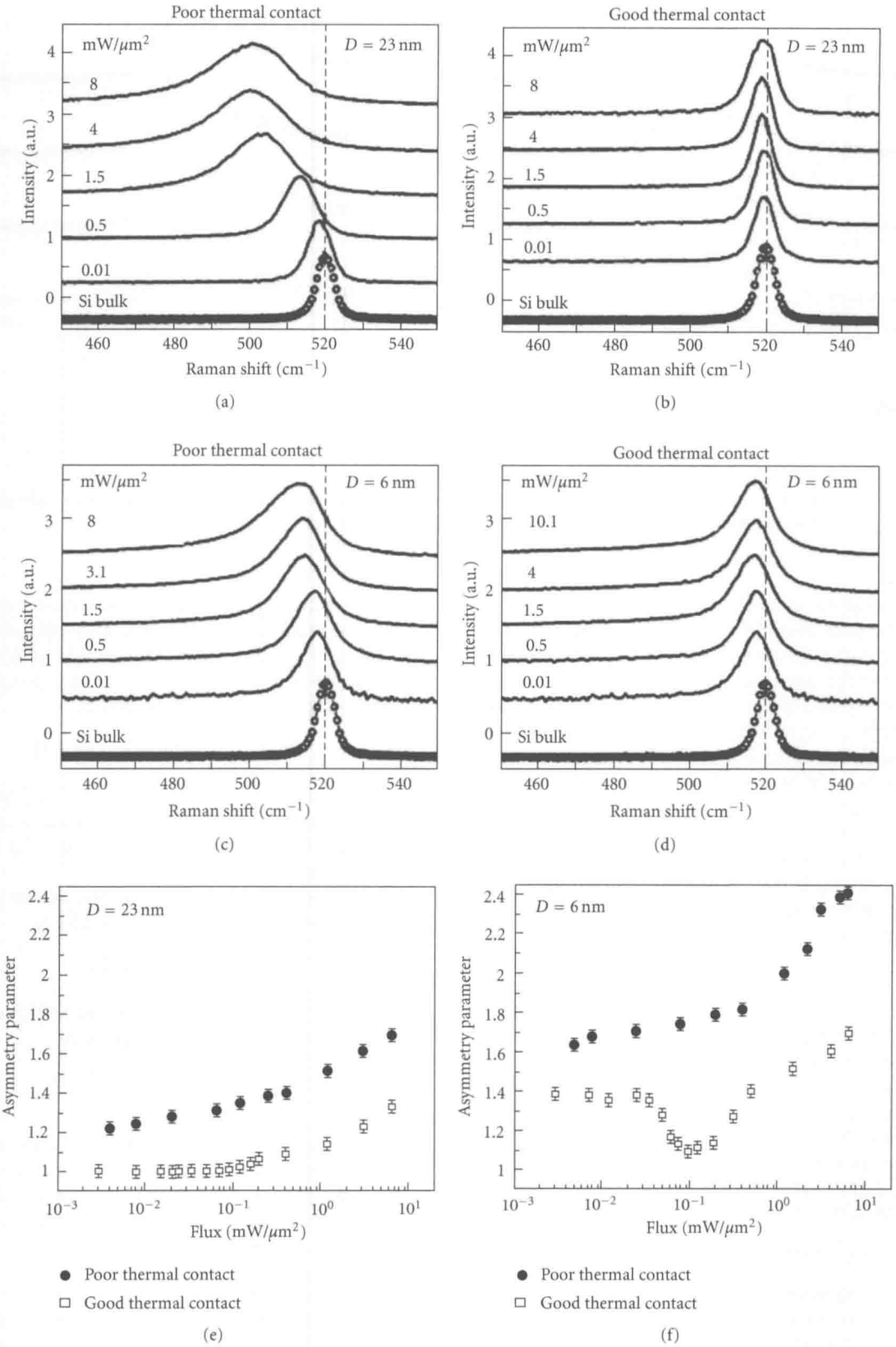

FIGURE 10: Flux (Φ) dependent Raman spectra of Si nanowires collected under poor thermal anchorage (a, c) and good thermal anchorage (b, d) for 23 nm wires (a, b) and 6.0 nm wire (c, d). The nanowires were located on an Indium substrate. (b) Flux (Φ) dependence of the asymmetry parameter A for Si nanowires under poor thermal contact (solid circles) and good thermal contact (open squares) for (e) 23 nm (f) 6.0 nm Si nanowires [46].

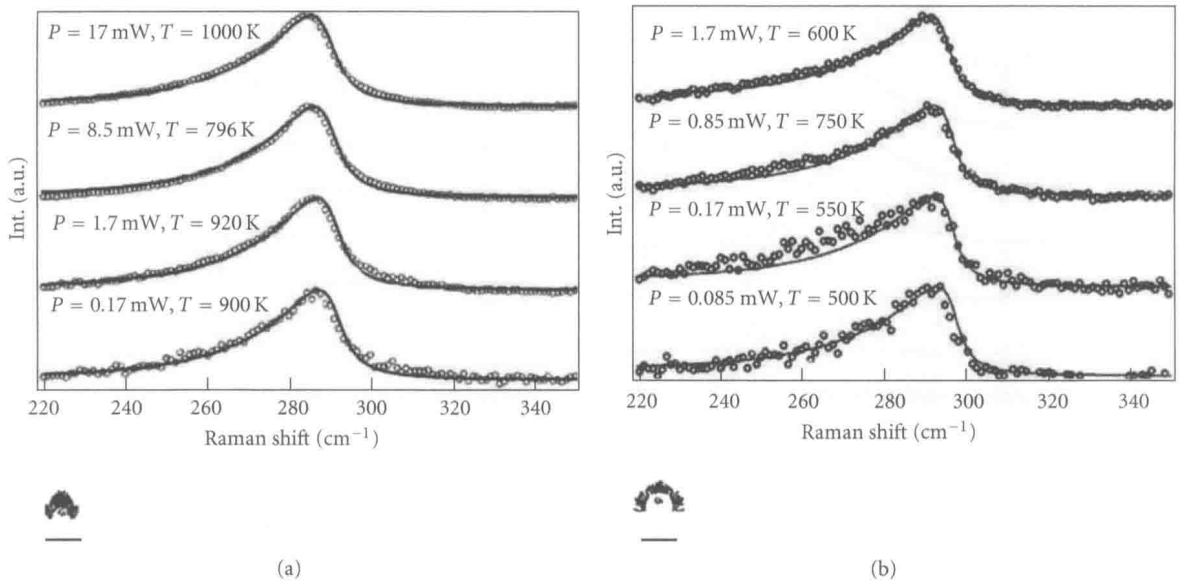

FIGURE 11: Raman spectra at 632.8 nm for the Ge nanowire ($D = 7$ nm) for varying laser power levels (circles) at two different Ga droplet sizes (a) droplet size ~1 μm and (b) droplet size ~1 mm. The solid lines represent the least square fit (10) [80].

thermal contact of the nanowire to the substrate and intense focusing of the laser beam in a micro Raman spectrometer can lead to significant heating of the sample. In this section, we discuss the temperature dependence of the first-order Raman spectra of Ge and Si nanowire due to variation in laser power and thermal conductance of the nanowire on the substrate. The subtle interplay between quantum phonon confinement and the local heating effect are shown to influence both the frequency shift and the asymmetric broadening of the Raman spectra.

The Stokes-anti-Stokes intensity ratio of first-order Raman spectra is normally used to determine the local temperature of the nanowire sample. The intensity ratio relates to the temperature by

$$\frac{I_s}{I_{as}} = P_o \exp\left(\frac{\hbar\omega_o}{k_B T}\right), \tag{4}$$

where ω_o is the phonon frequency, the prefactor P_o depends on the absorption constant and the Raman cross-section at a given frequency. Typically, the value of P_o is determined by calculating the Stokes-anti-Stokes intensity ratio I_s/I_{as} at room temperature and at the lowest possible laser power to eliminate any laser-induced heating. The phonon confinement function (3) is modified to include temperature dependence [128–130]. The frequency is expressed as

$$\omega(q, T) = \omega(q) + \Delta\omega_1(T) + \Delta\omega_2(T), \tag{5}$$

$\Delta\omega_1(T)$, is the frequency shift due to phonon decay processes. This phonon-phonon coupling term describes the anharmonic coupling between phonons and is approximated by

$$\Delta\omega_1(T) = A_1\left(1 + \frac{2}{x}\right) + A_2\left[1 + \frac{3}{x} + \left(1 + \frac{3}{x^2}\right)\right], \tag{6}$$

where $x = e^{(\hbar\omega_o/2\kappa_B T)} - 1$. The first term describes the coupling of the phonon to decayed low-energy two phonons (three-phonon coupling), and the second term describes the coupling to three decayed phonons (four-phonon coupling). A_1 is adjusted to match the bulk Ge and Si values. $\Delta\omega_2(T)$ is the frequency shift due to the thermal expansion of the lattice. The compressive stress expressed as

$$\Delta\omega_2(T) = \omega_o\{\exp(3\gamma\beta T) - 1\} \tag{7}$$

is neglected since the Si and Ge nanowires used in the studies exhibit limited or no oxide sheath formation as evidenced by Figure 8. γ is the Gruneisen parameter, and β is the thermal expansion coefficient of Ge or Si.

The temperature dependence of the inverse phonon life time (FWHM) in the formalism [128–130] is

$$\Gamma(T) = \Gamma + \Delta\Gamma(T), \tag{8}$$

where Γ is the FWHM of the bulk Ge or Si including the instrumental broadening, and $\Delta\Gamma$ is given as

$$\Delta\Gamma(T) = B_1\left(1 + \frac{2}{x}\right) + B_2\left[1 + \frac{3}{x} + \left(1 + \frac{3}{x^2}\right)\right], \tag{9}$$

where x is as defined previously. The first term is due to the three-phonon coupling, and the second term is the result of the four-phonon coupling effect on the FWHM of the Raman spectrum. Just as before, we neglect the four-phonon coupling term, and B_1 is adjusted to match the bulk Ge or Si values.

The asymmetric broadening of the Raman TO band has been attributed to Fano interference between scattering from the discrete optical phonon and an electronic continuum due to photon-excited charge carriers [126]. At sufficient doping levels, electrons and holes in semiconductors participate in inelastic scattering leading to Fano resonance. An asymmetry of the Fano line shape depends on the electron-phonon coupling strength. Attributable to the observation of asymmetry in the low-frequency tail, the contribution of Fano